International Journal of Statistics and Applied Mathematics 2019; 4(6): 01-13

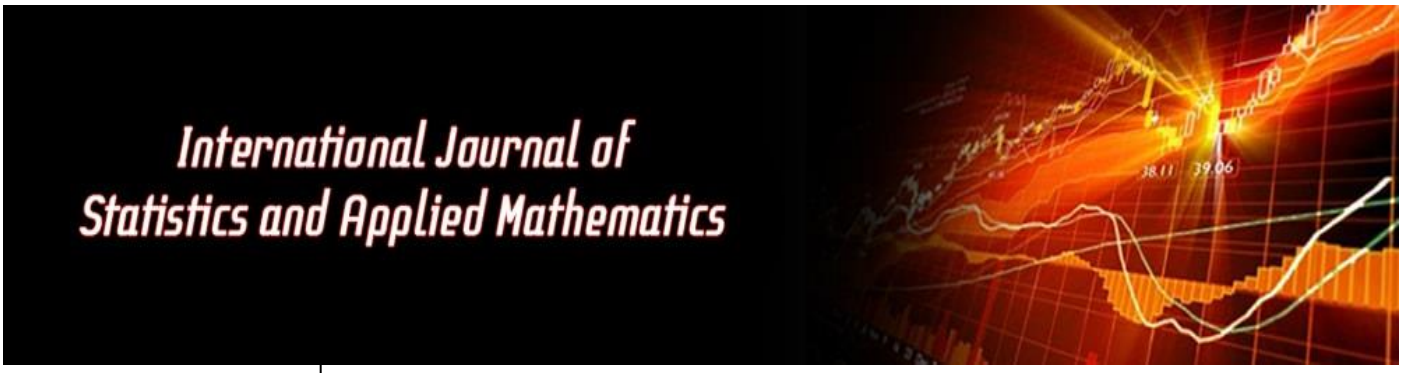

ISSN: 2456-1452
Maths 2019; 4(6): 01-13

www.mathsjournal.com
Received: 01-09-2019
Accepted: 03-10-2019

S Huq
Department of Mathematics, Bangladesh University of Engineering & Technology, Dhaka-1000, Bangladesh

MM Rahman
Department of Mathematics, Bangladesh University of Engineering & Technology, Dhaka-1000, Bangladesh

MF Karim
Department of Mathematical and Physical Sciences, East West University, Dhaka-1212, Bangladesh

MR Amin
Department of Mathematical and Physical Sciences, East West University, Dhaka-1212, Bangladesh

Corresponding Author:
MF Karim
Department of Mathematical and Physical Sciences, East West University, Dhaka-1212, Bangladesh

Computational study of natural convection in a rectangular porous enclosure with partially active wall in different heater and cooler positions

S Huq, MM Rahman, MF Karim and MR Amin

Abstract
Natural convection heat transfer and fluid flow through a two-dimensional rectangular porous enclosure with partially active thermal walls are investigated numerically in this study. A small part of two sidewalls are partially cooled at a constant temperature θ_c and a small part of the bottom wall is kept at constant temperature θ_h ($\theta_h > \theta_c$), where the top and the remaining part of the bottom wall and the side walls of the enclosure are assumed to be insulated. The physical problems are presented mathematically by different sets of governing equations (such as the mass, momentum and energy balance equations) along with the corresponding initial and boundary conditions by using Brinkman-Forchheimer-extended Darcy flow model and the Boussinesq approximation. Galerkin weighted residual method of finite element analysis is implemented to discretise the governing equations. The analysis has been carried out for the cavity Aspect ratio (*Ar* = 1, 2, 3), the three positions of heating source: left position (*Lp*), middle position (*Mp*), right position (*Rp*) and the three positions of cooling source: top cold (*Tc*), middle cold (*Mc*), and bottom cold (*Bc*) with various heater length and fixed Darcy number (*Da*), Porosity (ε), Prandtl number (*Pr*) for two values of Grashof number ($Gr = 10^5, 10^6$) with respect to time (τ). Results are presented in terms of isotherms, streamlines, average Nusselt number along the partially active thermal wall for different combinations of the governing parameters. The results indicate that both the flow and the thermal fields strongly depend on the above-mentioned parameters. The computational results also indicate that the average Nusselt number at the heated part of active wall with respect to time are depending on the aforementioned parameters. The results in terms of average Nusselt number are also shown in tabular form.

Keywords: Finite element method (FEM), location and length of heater, rectangular tall cavity, natural convection and porous enclosure

1. Introduction
Interest in natural convection fluid flow and heat transfer in porous media has been motivated by a large number of technical applications, such as, fluid flow in geothermal reservoirs, separation processes in chemical industries, dispersion of chemical contaminants through water saturated soil, solidification of casting, migration of moisture in grain storage system, crude oil production etc.
[1-6]. Comprehensive literature survey concerned with this subject is given [1-3]. The effects of aspect ratio and different thermal boundary conditions on the natural convection in a rectangular porous cavity have been studied numerically by Bhuvaneswari *et al.* [4]. Cheikh *et al.* [5] investigated the natural convection in an air-filled 2D square enclosure heated with a constant source from the bottom and with different configurations of sink on other walls. Mahmud and Faster [6] investigated the magneto hydrodynamic free convection and entropy generation in a square porous cavity. They found that the fluid velocity is reduced with the increase of the value of Hartmann number. Xu and Saha [7] studied the transition to an unsteady flow due to an adiabatic fin on the sidewall of a square cavity. Prasad and Kulacki [8] numerically studied the convection of heat transfer in a rectangular porous enclosure. It is observed from their results that the heat transfer rate increases with the increasing of aspect ratio. Varol *et al.* [9] numerically studied natural convection flow in a porous rectangular enclosure with a sinusoidaly varying temperature profile on the bottom wall.

They found that the heat transfer increases with the increase of amplitude of the sinusoidal function and decreases with the increase of Aspect ratio. Natural convection of heat transfer in a partially cooled and inclined rectangular porous enclosure have been investigated numerically by Öztop [10]. Author found that the heat transfer increases with the increase of Rayleigh number and this number is the dominant parameter on heat transfer and fluid flow as well as Aspect ratio. The authors Chamkha and Ismael [11], Khatun *et al.* [17] investigated the natural convection in differentially heated partially porous layered cavities for nano fluid. Saeid and Pop [12] investigated the natural convection in a square porous cavity with differential isothermal vertical walls and adiabatic horizontal walls. The results show that the effect of the inertia parameter on the fluid circulation in the porous cavity for different values of Rayleigh number. Nithiarasu *et al.* [13] described computationally the effect of natural convection on heat transfer in a porous cavity of same dimensions of Saeid [12]. Rathish and Kumar [14] analyzed numerically the natural convection in a fluid saturated porous trapezoidal enclosure of side wall heating under Darcian / Non-Darcian assumptions. The limitation of the Darcy-Brinkman-Forchheimer extended model are studied in [15].

Based on the above literature review, it appears that a very little work reported on the flow structure and the corresponding heat transfer in a partially heated and cooled porous enclosures. The objective of this present study is to analyse the effects of physical parameter of the structure in the temperature, fluid flow and average heat transfer rate.

2. Physical Configuration and Mathematical Formulation

Consider a two-dimensional rectangular enclosure of height *H* and width *L* filled with fluid saturated porous medium (as shown in Fig. 1). A little portion of the left and right walls of length H/2 of the enclosure is partially cold at a constant low temperature. A little portion of the bottom wall is kept at a constant high temperature. The top wall and the remaining part of the enclosure are assumed to be perfectly insulated. The fluid in the enclosure is incompressible and Newtonian. The gravity acts in the negative *y*-direction. The porous medium is assumed to be isotropic, homogeneous and in thermodynamic equilibrium with the fluid. In this study, the thermal properties of the fluid are kept constant except the density in the buoyancy term. The density varies linearly with temperature as $\rho = \rho_0[1 - \beta(\theta - \theta_0)]$, where β being the coefficient of thermal expansion and subscript 0 denoting the reference state. The Forcheimmer-Brinkman extended Darcy Model has been used to solve the governing equations.

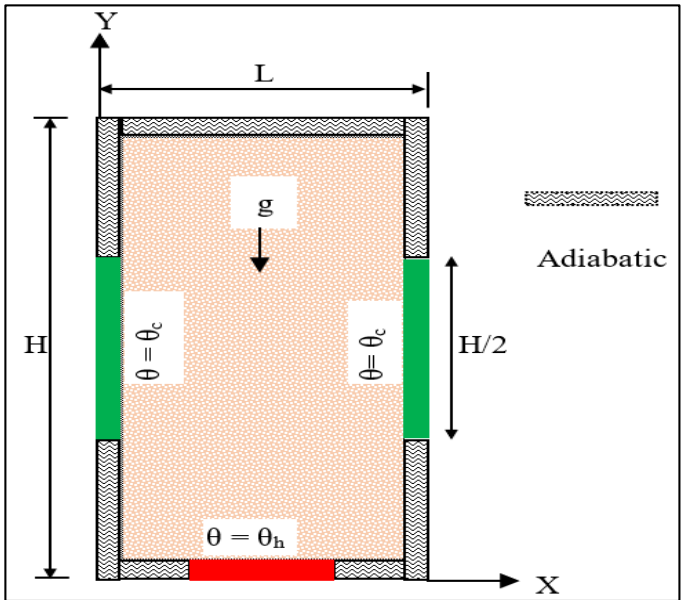

Fig 1: Schematic diagram of the physical model and boundary along with the coordinate system

According to above-mentioned assumptions, the governing equations for unsteady two-dimensional natural convection flow in a porous enclosure using conservation of mass, momentum and energy can be written with the following dimensionless forms:

$$\frac{\partial U}{\partial X} + \frac{\partial V}{\partial Y} = 0 \tag{1}$$

$$\frac{1}{\varepsilon}\frac{\partial U}{\partial \tau} + \frac{1}{\varepsilon^2}\left[U\frac{\partial U}{\partial X} + V\frac{\partial U}{\partial Y}\right] = -\frac{\partial P}{\partial X} + \frac{1}{\varepsilon}\nabla^2 U - \frac{U}{Da} - \frac{C_f}{\sqrt{Da}}U\sqrt{U^2+V^2} \tag{2}$$

$$\frac{1}{\varepsilon}\frac{\partial V}{\partial \tau} + \frac{1}{\varepsilon^2}\left[U\frac{\partial V}{\partial X} + V\frac{\partial V}{\partial Y}\right] = -\frac{\partial P}{\partial Y} + \frac{1}{\varepsilon}\nabla^2 V - \frac{V}{Da} - \frac{C_f}{\sqrt{Da}}V\sqrt{U^2+V^2} + GrT \tag{3}$$

$$\frac{\partial T}{\partial \tau} + U\frac{\partial T}{\partial X} + V\frac{\partial T}{\partial Y} = \frac{1}{\mathrm{Pr}}\nabla^2 T \tag{4}$$

where $C_f = \frac{1.75}{\sqrt{150\varepsilon^{3/2}}}$. The parameters C_p, g, K, p, t, α, ν, ε and σ are the specific heat, acceleration due to gravity, permeability of the porous medium, pressure, time, thermal diffusivity, kinematic viscosity, porosity of the medium and specific heat ratio, respectively.

The transformed initial and boundary conditions for the problem can be written as follows:

when $\tau = 0$, for the entire domain: $U = V = 0$, $T = 0$;

when $\tau > 0$, at the top wall: $U = V = 0$, $\partial T/\partial N = 0$;

At left and right walls: $U = V = 0$, $T = 0$ (on the cooling part); and $U = V = 0$, $\partial T/\partial N = 0$ (on the uncooling part);

At the bottom wall: $U = V = 0$, $T = 1$ (on the heater); and $U = V = 0$, $\partial T/\partial N = 0$ (on the unheated part);

where N is the non-dimensional distances either along X or Y direction acting normal to the surface.

The dimensional quantities appeared in the equations are simplified by the non-dimensional numbers. The nondimensional parameters appeared in the study are the Aspect ratio $Ar = H/L$, the Grash of number $Gr = \frac{g\beta\Delta TL^3}{\nu^2}$, the Prandtl number $Pr = \nu/\alpha$ and the Darcy number $Da = K/L^2$.

The heat transfer rate across the enclosure is an important parameter in the thermal engineering applications. It is defined by the Nusselt number along the hot wall of the cavity. The average Nusselt numbers at the heating portion of the left wall of the cavity are expressed as $Nu_{av} = -\frac{1}{\ell_h}\int_0^{\ell_h/L}\frac{\partial T}{\partial Y}\,dX$ where ℓ_h is the length of the heating portion and the non-dimensional stream function is defined as: $U = \frac{\partial \psi}{\partial Y}, V = -\frac{\partial \psi}{\partial X}$

3. Numerical Implementation

The nonlinear governing partial differential equations, i. e, mass, momentum and energy equations are transferred into a system of integral equations by using the Galerkin weighted residual finite element method. Details of the method are described in Zienkiewicz & Taylor [16]. The integration involved in each term of these equations is performed by using Gauss's quadrature method. Newton's method is used to modify the non-linear algebraic equations into linear equations with the help of the boundary conditions. Then finally we use Triangular Factorization method to solve these linear equations.

4. Code Validation

A comparison of streamlines and isotherms between Bhuvaneswari *et al.* [4] and present study for $Gr = 10^6$, $Ar = 3$, $\varepsilon = 0.2$ and $Da = 10$ is presented in Fig. 2. This figure shows that agreement between them is good.

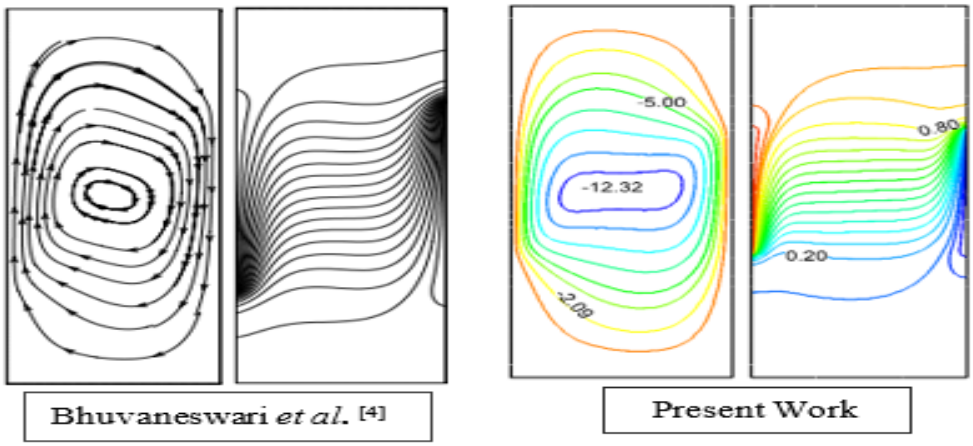

Fig 2: Streamlines (left) and isotherms (right) for Middle–Middle heating location with $Gr = 10^6$, $Ar = 3$, $\varepsilon = 0.2$ and $Da = 10^{-3}$

5. Result and Discussion

5.1 Effect of Aspect ratio

Figures 3 – 7 represents the isotherms, streamlines and average heat transfer rate for different aspect ratio inside a partially heated rectangular cavity filled with a porous medium with respect to time $\tau = 0.1$ and 1.0 for fixed $Gr = 10^5$ and 10^6. Three different aspect ratio (Ar) are chosen as 1, 2 and 3. The values of ε, Pr, Da and ℓ_h are fixed at 0.3, 0.7, 10^{-3} and 0.4 respectively, while heater is located at the middle position (Mp) of the bottom wall and cooling sector is located at the middle-cold (Mc) position of the vertical walls. The aspect ratio is the ratio of the height H and length L.

Figure. 3 illustrates the isotherm contour in porous enclosure for abovementioned case with respect to time $\tau = 0.1$ and 1.0 for a fixed Grashof number, $Gr = 10^5$. In this configuration at both the time $\tau = 0.1$ and 1.0, for aspect ratios ($Ar = 1$, 2) smooth, symmetrical, parabolic temperature patterns are observed and for $Ar = 3$, it remains no longer parabolic. For $Ar = 1$, isothermal line starts to turn back towards horizontal active wall and at $\tau = 0.1$, there was just two thermal lines are not parabolic, which almost parallel to vertical wall and also few more parallel lines exist for $\tau = 1.0$. But this type of thermal line does not exist for other higher aspect ratios. It is seen that for higher value of Ar, most of the isothermal lines turn back towards vertical cold walls at $\tau = 0.1$ and 1.0. On increasing the aspect ratio, the fluid in the upper parts of the enclosure is stagnant due to increasing the

space of the enclosure. It may be noted that the heat lines are smooth and symmetric for all *Ar* and these heat lines disperse near the thermal active wall. The isotherms indicate that the heat is distributed well in the enclosure for all aspect ratios.

Figure 4 shows the isotherm contour for different aspect ratios with respect to time τ = 0.1 and τ = 1.0 for $Gr = 10^6$. The isothermal lines move from bottom to top along cold boundary confined in the side wall indicating a vigorous convection at τ = 0.1 and at τ = 1.0, the changes of flow patterns are negligible. It is seen from the corresponding isotherms that the large temperature gradient characterizes the region immediately adjacent to the thermally active wall locations while negligible gradients (upper part of the hot/cold wall location) prevail in the rest of the cavity. Almost same pattern is observed for all aspect ratios at $Gr = 10^6$. A single thermal line exists which is almost parallel to the vertical wall for higher (*Ar* = 2,3) at both the time τ = 0.1 to 1.0. On increasing with time, the parallel line moves to upper side of vertical wall. But the line does not exist for low aspect ratio, *Ar* = 1. Hence, this is clearly seen from the corresponding isotherms that the heat distributions show the different patterns on the shallow cavity and the vertical cavity.

Figure 5 demonstrates the flow field at τ = 0.1 to 1.0 which remains almost identical for all values of *Ar* for $Gr = 10^5$. It is seen that the streamline shows two counter rotating vortex which is the result due to the action of the buoyant forces that generated by the fluid temperature differences and cause the fluid to rise in the middle and to descend on the sides of the enclosure at τ = 0.1 and 1.0 and also seen from these figures that the vortex become large in size and contour value is decreasing with increasing *Ar* for both time τ = 0.1 and 1.0. There is also a major change in the flow field for *Ar* = 3 with increasing the time τ = 1.0, the primary vortex remains unchanged and two secondary clock-wise rotating cells are developed at the top and bottom corner near the right wall due to increasing the height of the enclosure. It is observed from figure that the contour value is decreasing with increasing of *Ar* indicating a sign of reign on natural convection in the porous cavity.

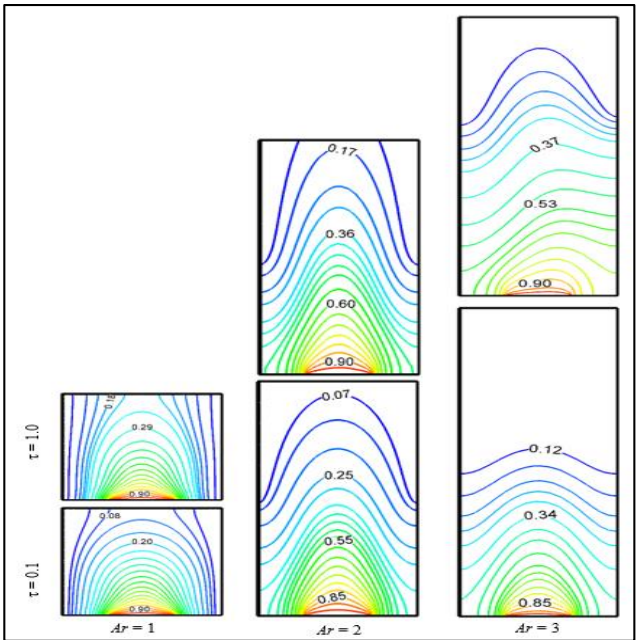

Fig 3: Isotherm contours for different *Ar* at $Gr = 10^5$ and $Da = 10^{-3}$, ε = 0.3, ℓ_h = 0.4.

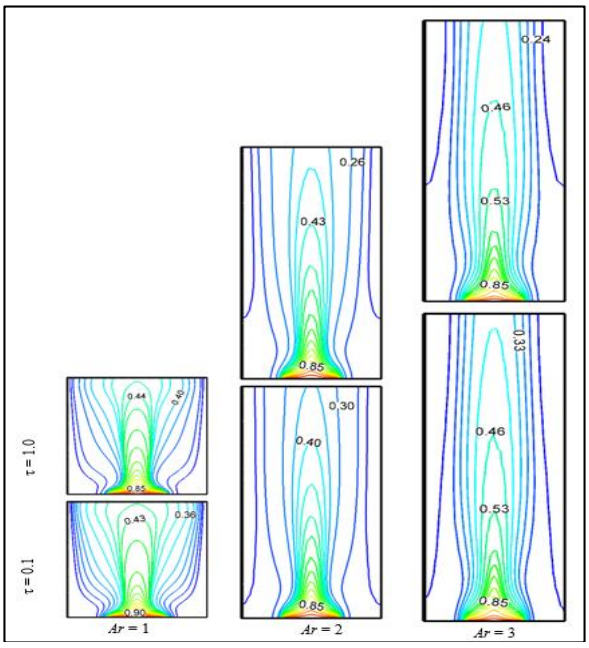

Fig 4: Isotherm contours for different *Ar* at $Gr = 10^6$ and $Da = 10^{-3}$, ε = 0.3, ℓ_h = 0.4.

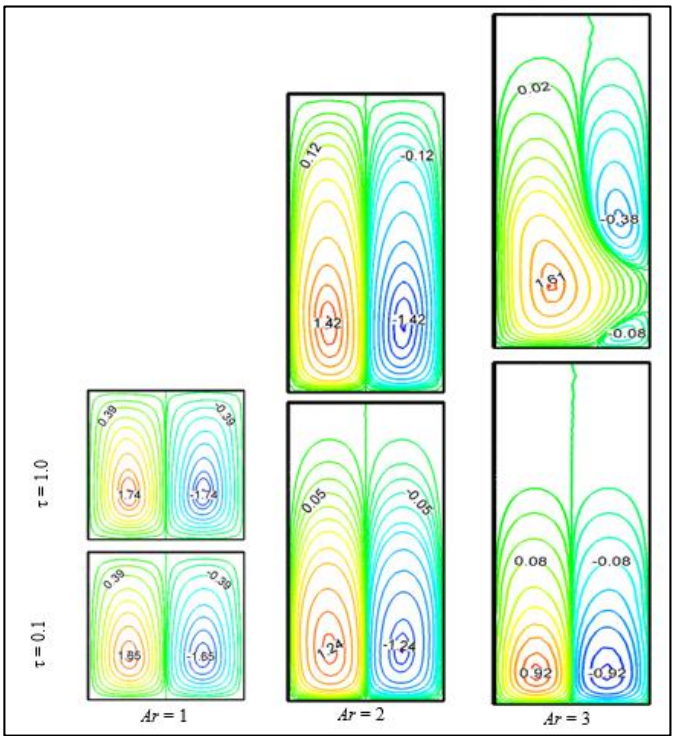

Fig 5: Streamline contours for different *Ar* at $Gr = 10^5$ and $Da = 10^{-3}$, $\varepsilon = 0.3$, $\ell_h = 0.4$.

Figure 6 displays the streamlines for different values of aspect ratio for $Gr = 10^6$. Multiple primary and secondary vortices rotating in opposite directions to each other are formed within the rectangular cavity at $\tau = 0.1$ and 1.0. Clockwise and anti-clockwise flows are shown via negative and positive signs of stream functions is observed for all aspect ratios. On increasing the aspect ratio, the fluid in the upper parts of the enclosure is stationary due to inactive upper zone and flow strength is enlarged at both the time $\tau = 0.1$ and 1.0 due to strong buoyancy effect for higher *Gr*. It can be realized from figure that the contour value of core region is increased by increasing of *Ar* with respect to time and also may be seen that contour value of core region is higher at *Ar* =2 than *Ar* = 3 due to increasing the height of the cavity.

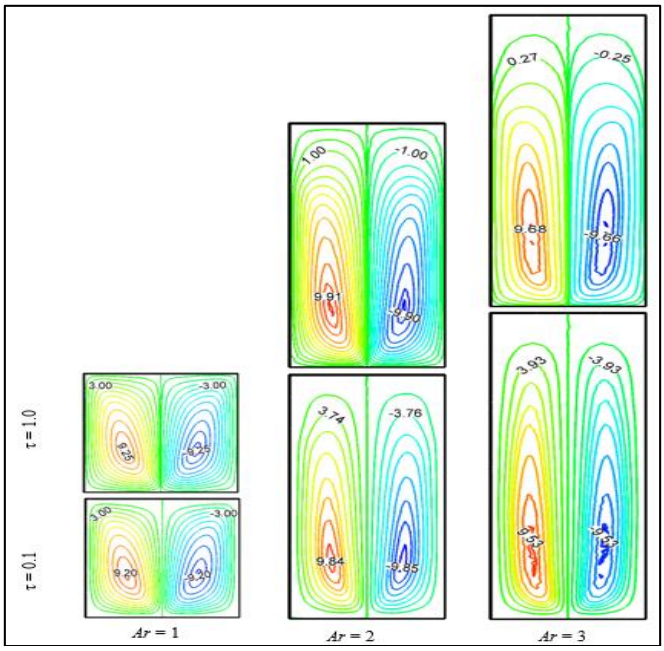

Fig 6: Streamline contours for different *Ar* at $Gr = 10^6$ and $Da = 10^{-3}$, $\varepsilon = 0.3$, $\ell_h = 0.4$.

Also, it may be observed from Figures 3 to 6 that the effect of *Gr* for fixed value of the aspect ratio *Ar*, with the increase of *Gr* the heated floor exerts more influence in the flow field along the cavity height and isotherm lines tend to be compressed from the heated wall. When the cavity height increases, higher values of *Gr* are necessary for the establishment of a thermal line near the cold vertical wall. In the range of lower values of *Gr* and higher values of *Ar*, the thermal line is not maintained. As the Grashof number increases, the intensity of convection intensifies within the cavity due to the increase in buoyancy effect which generated by temperature difference. This is evident from the substantial increase in the flow circulation within the cavity at different times.

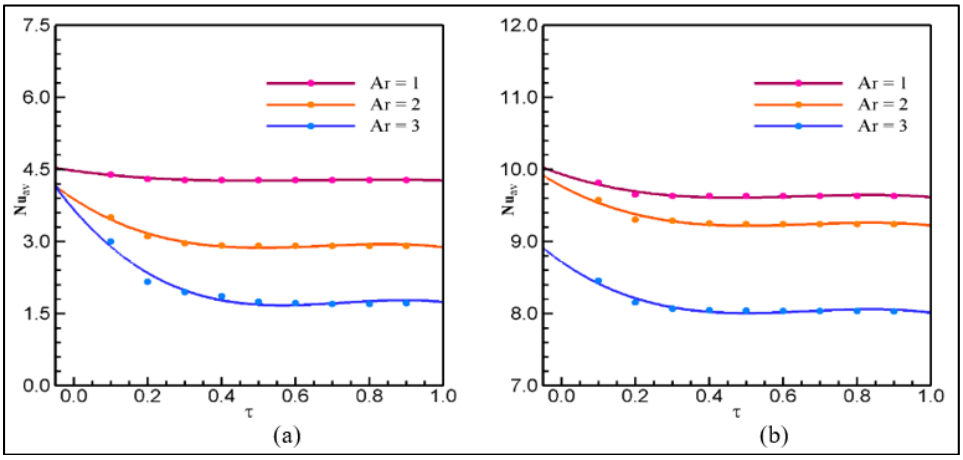

Fig 7: Variation of average Nusselt number with time for different *Ar* on the heated wall at (a) $Gr = 10^5$ and (b) $Gr = 10^6$.

Figures 7(a) and (b) express the average Nusselt number at the heated part of the bottom wall in different Aspect ratio with above mentioned case with respect to time for $Gr = 10^5$ and $Gr = 10^6$ respectively. The graph shows that the regression line of the average Nusselt number with respect to time which provides the best fit to the specific curves in the dataset. An overview of the figure reveals that the value of the average Nusselt number smoothly decreases steadily with time for $Ar = 2, 3$ at both $Gr = 10^5$ and 10^6. But for $Ar = 1$, the Nu_{av} gives almost constant value at both $Gr = 10^5$ and 10^6. In addition, the heat transfer rate gives minimum value for higher Aspect ratio, $Ar = 3$ and in particular, it is also observed that the value of average Nusselt number is significantly higher with the increasing the value of *Gr* due to the enhanced convection for all the cases of *Ar*. Hence the higher heat transfer rate is obtained at the homogeneous porous medium.

Table 1: Variation of average Nusselt number with respect to Time τ for different aspect ratio.

τ	Nu_{av}			Nu_{av}		
	$Gr = 10^5$			$Gr = 10^6$		
	$Ar = 1$	$Ar = 2$	$Ar = 3$	$Ar = 1$	$Ar = 2$	$Ar = 3$
0.1	4.334527	3.374132	3.155021	9.668892	9.505738	8.454741
0.3	4.277792	2.919846	1.962343	9.628444	9.244618	8.066341
0.5	4.277285	2.909911	1.744317	9.628364	9.239076	8.03856
0.7	4.27696	2.909074	1.701886	9.628375	9.238825	8.034076
1.0	4.277379	2.908949	1.798237	9.62831	9.238886	8.0322

5.2 Effect of Heater Position

In many situations, a heat transfer designer prefers to avoid the use of mechanical fans or other active equipment's for fluid circulation, due to power consumption, excessive operating noise or reliability concerns. Hence, the placement of these heaters within the enclosure requires to be optimized so as to maximize the heat removal from the heater to the adjacent fluid. Consequently, in this section, the location of the heater was considered as a parameter and results are exposed in Figures 8–12. The isotherms, streamlines and average heat transfer rate inside a partially heated rectangular cavity filled with porous medium are shown in these figures. Three different Location of heater are chosen as *Lp* (left-position), *Mp* (middle-position) and *Rp* (right-position). In this case, the values of *Ar*, *Pr*, ε, *Da* and ℓ_h are fixed at 2, 0.7, 0.5, 10^{-3} and 0.4 respectively. While cooling part is located at the top-cold (*Tp*) position of the vertical walls.

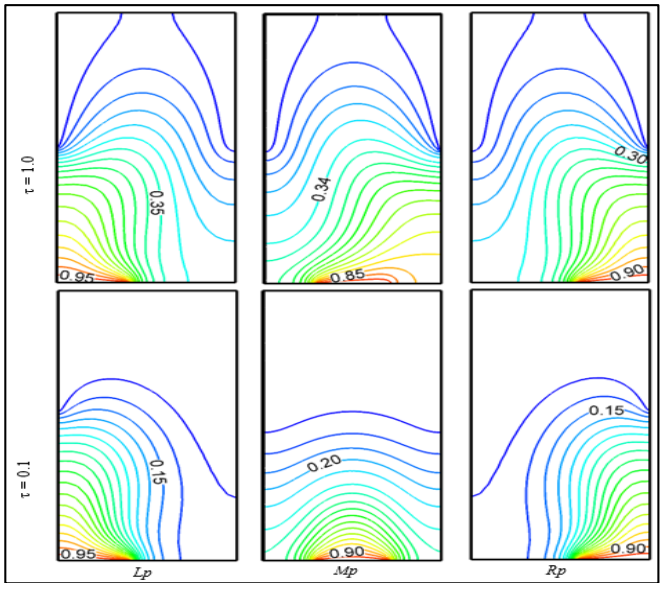

Fig 8: Isotherm contours for different position of heater at $Gr = 10^5$ and $\varepsilon = 0.5$, $Da = 10^{-3}$, $\ell_h = 0.4$.

Figure 8 shows the isotherm contours for different locations of the heater at time τ = 0.1 and 1.0, while ℓ_h = 0.4 and $Gr = 10^5$. It can be seen from the figure that at the middle position (*Mp)* of the heated bottom wall and top-vertical cold wall, the fluid rises from the heater due to low buoyancy, forming symmetric rolls and fluid flow becomes almost parallel to the top wall inside the cavity at τ = 0.1. It is also seen that at the left position (*Lp)*, the flow spirits on the way to upper part of the enclosure from the left corner position of the bottom wall. At time τ = 0.1, it is just lower half of the domain and the right position (*Rp)* is just the mirror image of *Lp* at both the time τ = 0.1 and 1.0. As increases time to τ = 1.0, thermal activity is intensified along the cold top part of the enclosure for $Gr = 10^5$ due to domination of conduction effects with higher porosity of the porous medium.

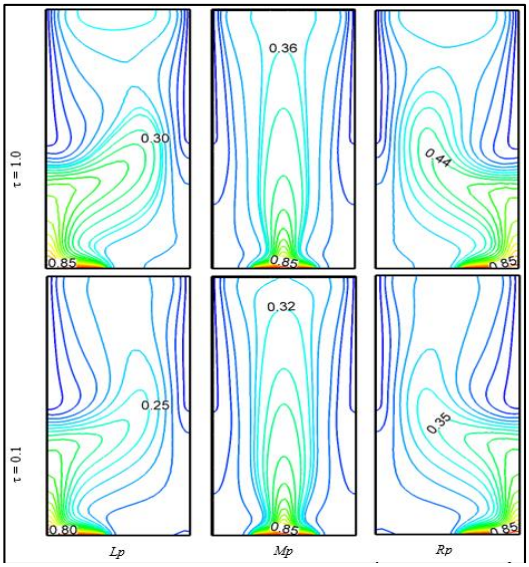

Fig 9: Isotherm contours for different position of heater at $Gr = 10^6$ and ε = 0.5, $Da = 10^{-3}$, ℓ_h = 0.4.

Figure 9 illustrates the isotherm contours for different locations of the heater at time τ = 0.1 and 1.0, while ℓ_h = 0.4 and $Gr = 10^{6.}$ It can be seen from the figure that as *Gr* increases to 10^6, the nonlinearity in the isotherms become higher and plume-like temperature distribution is observed for all different position with respect to time. Fluid rises from the heater on the bottom wall due to strong buoyancy forces, for the higher value of *Gr* at both the time τ = 0.1 and 1.0. This is clearly seen from the corresponding isotherms that *Lp* is a mirror image of *Rp* at both the time and two or more thermal lines start to develop near the cold walls which are almost parallel to the vertical walls for all positions. The physical reason behind this is that, at the highest Grashof number, natural convection is more effective than that of conduction wall. The isotherms indicate that the heat is distributed well in the enclosure for all different positions.

Figure 10 depicts the streamline contours for different location of heater for $Gr = 10^5$ at τ = 0.1 and 1.0. It is observed for *Mp*, clockwise and anti-clockwise flows are shown via negative and positive signs of stream functions, for *Lp*, clockwise flows with negative sign stream functions and for *Rp*, anti-clockwise flows with positive sign of stream functions at τ = 0.1. With increasing time, a single cell bifurcates into two counter rotating cells for *Lp* and *Rp* position. It is also observed from figure that a small anti-clockwise rotating cell is formed at the left top corner of the cavity for *Lp* and a small clockwise rotating cell is formed at the right top corner of the cavity for *Rp* and a small clockwise rotating cell is also formed at the right top corner of the cavity for *Mp*. Hence at τ = 0.1 flow strength are almost identical for *Mp* and *Rp*. This may be attributed to domination of conduction effects and the presence of porous medium.

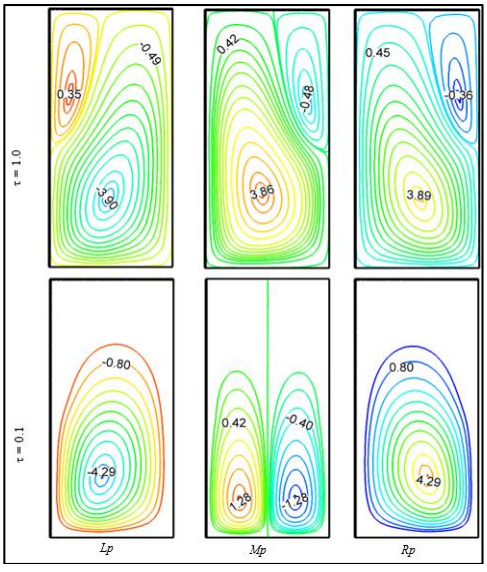

Fig 10: Streamline contours for different position of heater at $Gr = 10^5$ and ε = 0.5, $Da = 10^{-3}$, ℓ_h = 0.4.

Figure 11 describes the streamline contours for different locations of the heater at time τ = 0.1 and 1.0, while ℓ_h = 0.4 and *Gr* = $10^{6.}$ It can be seen from the figure that for the higher *Gr*, two counter rotating cells are detected for all different positions at both the time τ = 0.1 and 1.0. The pattern of the circulation cells is almost same for all different locations of the heater as stated earlier. A small rotating cell is designed at the left top corner of the cavity for *Lp* and right top corner for *Rp*. Two counter rotating symmetric cells with respect to a symmetric line are observed for *Mp* position. However, with the increase of Grashof number, *Gr*, natural convection becomes dominant; as a result, flow intensity increases and the circle shaped circulation cell becomes an elliptic shape for the different location of the heater considered. Finally, for the higher values of *Gr* to 10^6, there is a strong effect of buoyancy force in the flow and thermal field with respect to time for all positions of heater are observed from Fig. 8-11. Hence the location of heater suggestively affects the flow and temperature field.

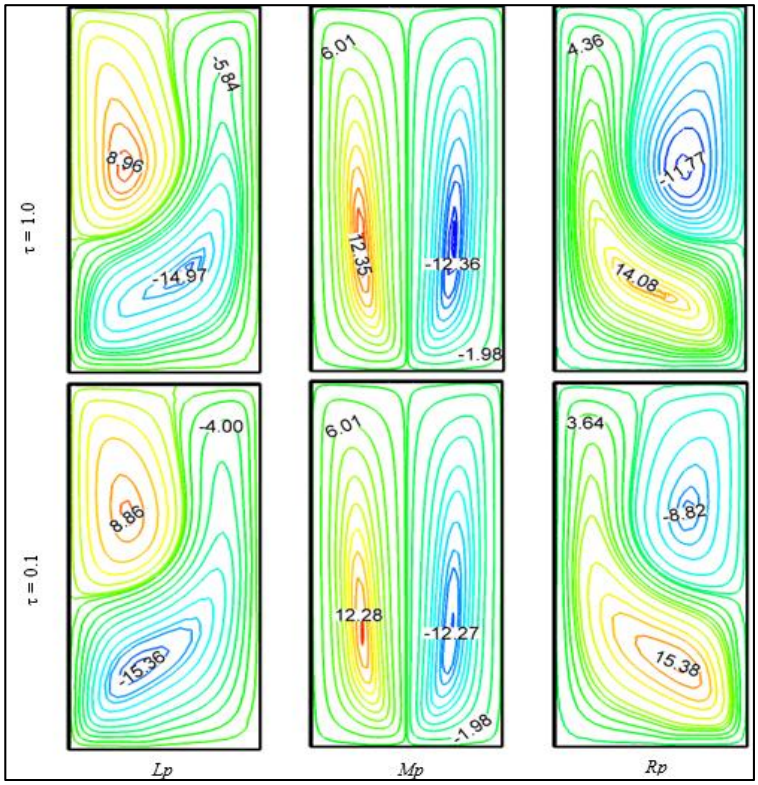

Fig 11: Streamline contours for different positions of heater at *Gr* = 10^6 and ε = 0.5, *Da* = 10^{-3}, ℓ_h = 0.4.

Figures 12 (a**)** and (b) depict the variation of the average Nusselt number Nu_{av} at the heated surface in the cavity for the aforementioned cases against Grashof number *Gr* for different locations of the heater. From this figure it is observed that when the value of *Gr* = 10^5 then the value of Nu_{av} for the middle position (*Mp*) is lower than other positions and the distribution of Nu_{av} smoothly decreases then increases with increasing τ. Left (*Lp*) and Right (*Rp*) position give almost similar value of Nu_{av} with respect to time. On the other hand, with the increasing of *Gr* at 10^6, the value of Nu_{av} for the middle position (*Mp*) is higher than other positions of the bottom wall. Up to a certain value of *Gr* the distribution of Nu_{av} smoothly decreases with increasing time. In this case the regression line for Left and Right position is relatively constant with respect to time. So, it is realized from the graph that the average heat transfer rate are increases with the increasing of the Grashof number because of strong effect of buoyancy force for all declared positions.

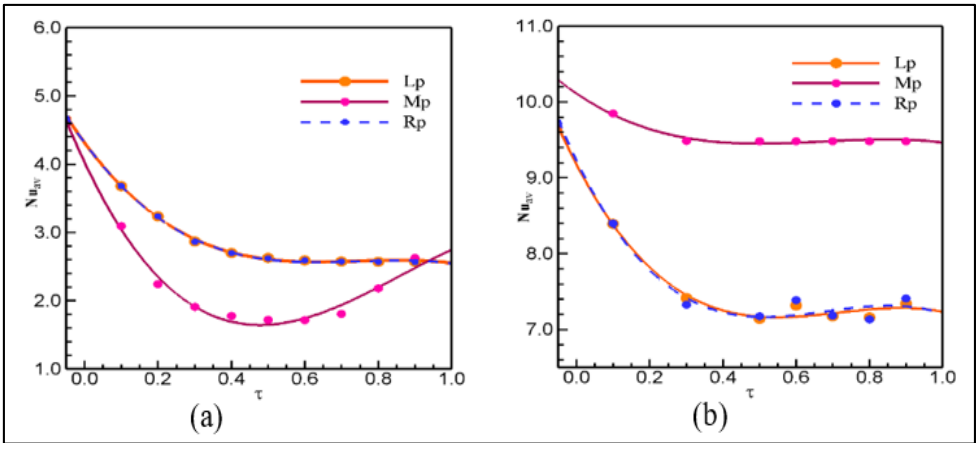

Fig 12: Variation of average Nusselt number with time for different location of heater on the heated wall at (a) *Gr* = 10^5 and (b) *Gr* = 10^6

Table 2: Variation of average Nusselt number with respect to Time τ for different Location of Heater.

τ	Nu_{av}			Nu_{av}		
	$Gr = 10^5$			$Gr = 10^6$		
	L_P	M_P	R_P	L_p	M_P	R_P
0.1	3.67858	3.091351	3.678482	8.393462	9.843578	8.395954
0.3	2.86401	1.907246	2.862438	7.414467	9.483943	7.327091
0.5	2.622996	1.719374	2.62214	7.139179	9.482699	7.172481
0.7	2.576068	1.80557	2.572376	7.173619	9.482619	7.184779
1.0	2.565202	2.685616	2.563792	7.233036	9.482706	7.202283

5.3 Effect of Cooling Segment Position

One of the fundamental problems in cooling of electronic devices is the optimal positioning of a distinct heat source in finite modular enclosures. Consequently, in this section, the location of the cooler segment was considered as a parameter and results are exposed in figures 13–17. The isotherms, streamlines and average heat transfer rate inside a partially heated rectangular tall cavity filled with in a porous medium are shown in these figures. Three different Location of cooler segment are chosen as *Tc* (top-cold), *Mc* (middle-cold) and *Bc* (bottom-cold) positions in the vertical walls. In this case, the values of *Ar*, *Pr*, *ε, Da* and ℓ_h are fixed at 2, 0.7, 0.5, 10^{-3} and 0.6 respectively. While heater is located at the middle position of the bottom wall.

Figure 13 shows the isotherm contours for different locations of the cooling portion to the vertical walls at time τ = 0.1 and 1.0, while ℓ_h = 0.6 and $Gr = 10^5$, it can be seen from the figure that in the position *Tc*, fluid rises from the partially heated bottom wall, forming a weak symmetric rolls and fluid flow becomes almost parallel to the top wall inside the half of the cavity at τ = 0.1 and nonlinear flow distribution entire the cavity is observed at τ = 1.0. In the position *Mc*, smooth parabolic shaped flow is shown at τ = 0.1 and flow strength are increased and also a single line is observed along the cold walls with the increasing of time. In the position *Bc*, a smooth, symmetrical parabolic shaped flow is observed which is along the heated bottom wall and two thermal line are observed along cold walls with the increasing of time to τ = 1.0 as shown in figure. This is because the inactive upper part of the enclosure.

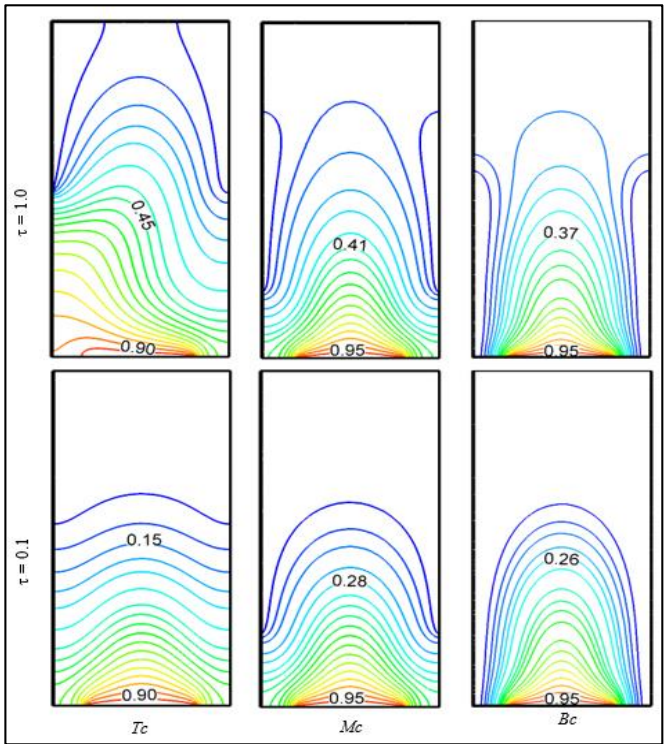

Fig 13: Isotherm contours for different Cold-position at the side walls for $Gr = 10^5$ and $\varepsilon = 0.5$, $Da = 10^{-3}$, $\ell_h = 0.6$.

Figure 14 illustrates the isotherm contours for different locations of cooling portion at time $\tau = 0.1$ and 1.0, while $\ell_h = 0.6$ and $Gr = 10^6$. It can be seen from the figure that as *Gr* increases to 10^6, the nonlinearity in the isotherms becomes higher and plume-like temperature distribution is observed for all different positions with respect to time. Fluid rises from the heater on the bottom wall due to strong buoyancy forces, for higher values of *Gr*. This is clearly seen from the corresponding isotherms that two or more thermal lines are starts to develop near the cold for position *Tc* and *Mc* at both time τ = 0.1 and 1.0. But in the position *Bc*, no line remains along cold bottom walls with time due to inactive upper part of the domain at both time τ = 0.1 and 1.0. The physical reason behind this is that, at the highest Grashof number, natural convection is more effective than that of conduction wall. The isotherms specify that the heat is dispersed well in the enclosure for all different cooler positions.

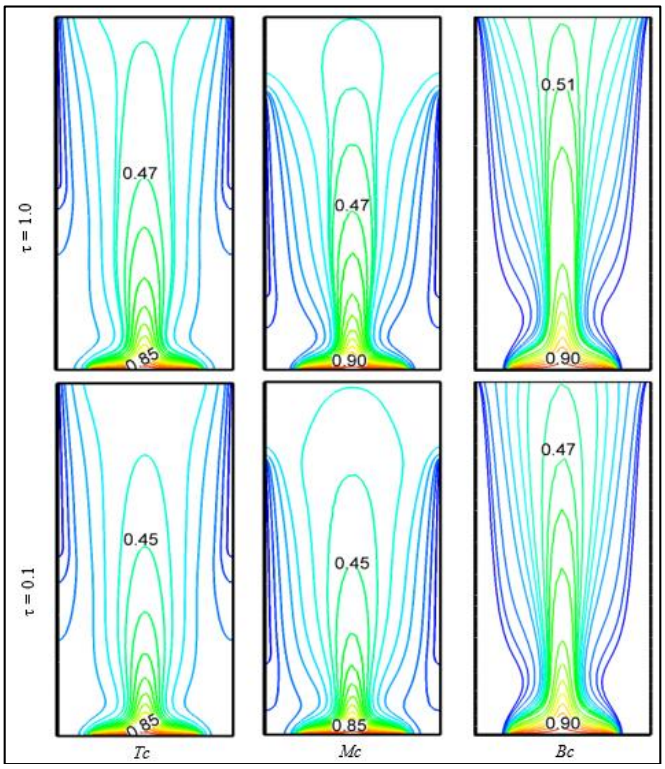

Fig 14: Isotherm contours for different cold-position at the side walls for $Gr = 10^6$ and $\varepsilon = 0.5$, $Da = 10^{-3}$, $\ell_h = 0.6$.

Figure 15 depicts the streamline contours for different location of cooling portion for $Gr = 10^5$ at $\tau = 0.1$ and 1.0. It is observed that for all considered locations, clockwise and anti-clockwise flows are shown via negative and positive signs of stream functions at $\tau = 0.1$. For *Tc*, anti-clockwise flows decrease with the increasing of time and a small rotating cell is observed in left-top position at $\tau = 1.0$. This is because of the top cold vertical walls. For *Mc* and *Bc*, flow strength become increased with the increasing of time to $\tau = 1.0$ for lower value of *Gr*. This may be attributed to domination of conduction effects and the presence of porous medium.

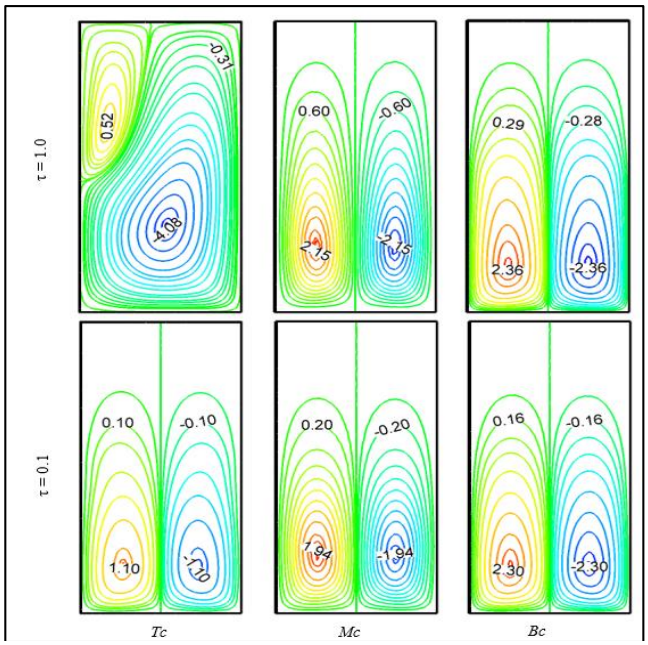

Fig 15: Streamline contours for different Cold-position at the side walls for $Gr = 10^5$ and $\varepsilon = 0.5$, $Da = 10^{-3}$, $\ell_h = 0.6$.

Figure 16 describes the streamline contours for different locations of cooling portion at time $\tau = 0.1$ and 1.0, while $\ell_h = 0.6$ and $Gr = 10^6$. It can be seen from the figure that for the higher *Gr*, two counter rotating cells are detected for all different positions at both time $\tau = 0.1$ and 1.0. The pattern of the circulation cells is almost similar for all different locations of cooling portion as stated earlier. In the position *Tc* flow circulation is higher at both time $\tau = 0.1$ and 1.0. When cooling section moves from top to bottom of the side walls, it is observed that flow circulation reduces and the contour value of the core region is also decrease. However, with the increasing of Grashof number, *Gr* natural convection becomes dominant; as a result, flow velocity increases and the circle shaped circulation cell becomes an elliptic shape for the different locations of cooling portion as considered. Finally, for the higher values of *Gr* to 10^6 there is a strong effect of buoyancy force in the flow field with respect to time.

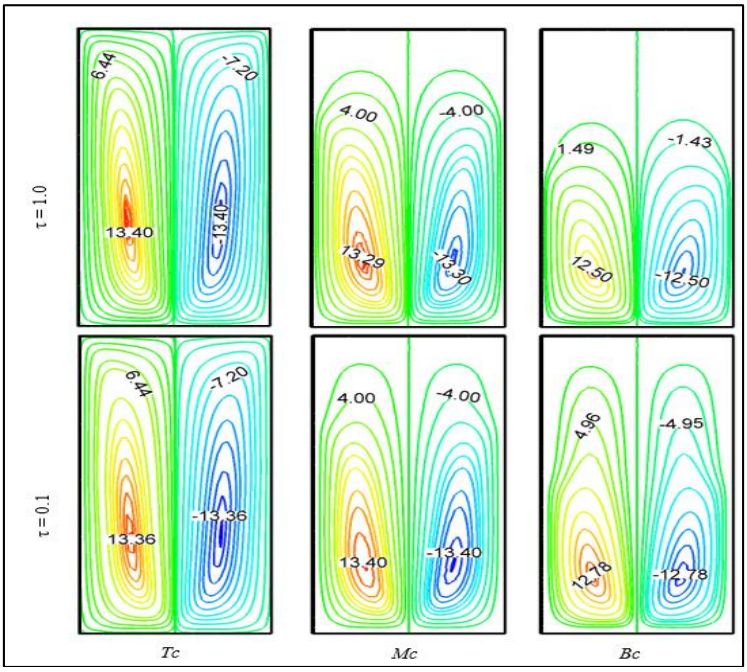

Fig 16: Streamline contours for different cold-position at the side walls for $Gr = 10^6$ and $\varepsilon = 0.5$, $Da = 10^{-3}$, $\ell_h = 0.6$.

Figures 17 (a**)** and (b) represent the variation of the average Nusselt number Nu_{av} at the heated surface with time in the cavity against Grashof number *Gr* for different locations of the cooler segment. From this figure it is observed that when cold portion is at the position *Tc* of the vertical walls, the value of Nu_{av} is lower than *Mc* and the value of Nu_{av} at *Mc* is lower than B_C respectively for all considered *Gr*. The regression line of *Mc* and *Bc* is relatively constant with respect to time for Gr = 10^5. The graph also shows that the value of average Nusselt number increases steadily with time for the position of cooler section is from *Tc* to *Bc* respectively for all considered *Gr*. It is also realized from the graph that the average heat transfer rate increases with the increasing of the Grashof number because of strong effect of buoyancy force for all declared position of cooler segment.

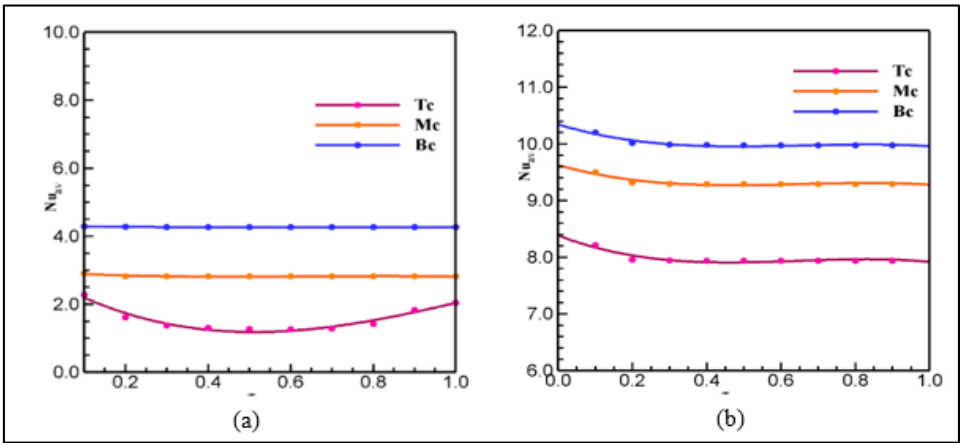

Fig 17: Variation of average Nusselt number with time for different locations of cooling section on the heated wall at (a) $Gr = 10^5$ and (b) $Gr = 10^6$.

Table 3: Variation of average Nusselt number with respect to Time τ for different Location of Cooling section.

τ	Nu_{av}			Nu_{av}		
	$Gr = 10^5$			$Gr = 10^6$		
	Tc	***Mc***	***Bc***	***Tc***	***Mc***	***Bc***
0.1	2.274564	2.902698	4.289838	8.217348	9.499795	10.204438
0.3	1.37863	2.818468	4.268062	7.9414	9.297235	9.986029
0.5	1.272497	2.81782	4.266395	7.940739	9.293043	9.976499
0.7	1.282011	2.817728	4.265565	7.940756	9.292684	9.974347
1.0	2.042896	2.817623	4.264888	7.940719	9.292589	9.973113

Nomenclature

Da	Darcy number	*Lp*	heater at left position
E	Porosity	*Tc*	cold temperature at top position
Pr	Prandtl number	Mc	cold temperature at middle position
Gr	Grashof number	Bc	cold temperature at bottom position
A_r	cavity aspect ratio	*Greek symbols*	
Nu_{av}	Average Nusselt number	μ	dynamic viscosity
T	dimensional time	v	kinematic viscosity
H	length of the cavity	α	thermal diffusivity
L	width of the cavity	C_f	forchheimer coefficient
T	dimensionless temperature	*K*	permeability
P	dimensional pressure	*h*	convective heat transfer coefficient
P	non-dimensional pressure	θ	dimensional temperature
ℓ_h	length of heater	ρ	density
x, y	dimensional coordinates	Ψ	stream function
X, Y	dimensionless coordinates	τ	dimensionless time
u, v	dimensional velocity components	*Subscripts*	
U, V	dimensionless velocity components	*av*	Average
Rp	heater at right position	*h*	Hot
Mp	heater at middle position	*c*	Cold

6. Conclusions

A computational work has been done using finite element method to investigate the unsteady natural convection flow and heat transfer in a rectangular porous enclosure with partially active thermal walls.

The following main concluding remarks are drawn from the present study:

a) The results of the numerical study carried out using the mathematical model and solution procedure proposed in this paper is fairly well when compared to the results of the benchmark case given in the literature.

b) The influence of cavity aspect ratio on fluid flow and temperature field is found to be pronounced. The heat transfer rate for higher cavity aspect ratio is lower than for lower aspect ratio.

c) The position of thermally active wall is a significant parameter of porous medium. The heat transfer rate for middle-position (*Mp*) is the best combination than other positions.

d) The value of average Nusselt number increases steadily with time for the position of cooler section is from *Tc* to *Bc* respectively for all considered *Gr*.

e) Heat transfer is increased with the increasing the Grashof number and higher fluid temperature is found for the highest value of the Grashof number.

7. Acknowledgements

The authors wish to acknowledge the technical support provided by the Department of Mathematics, Bangladesh University of Engineering and Technology (BUET), Dhaka-1000, Bangladesh.

8. References

1. Nield DA, Bejan A. Convection in porous media, 4th Edition, Springer Science and Business Media, New York, 2013, 778,
2. Vafai K. Handbook of porous media, 2nd Edition, Taylor & Francis, New York, 2005.
3. Md. Fayz-Al-Asad, Jahirul Haque Munshi M, Rajib Kumar Bhowmik, Sarker MMA. MHD free convection heat transfer having vertical fin in a square wavy cavity, Int. J. Stat. Appl. Math, 2019; 4(3):32-38,
4. Bhuvaneswari M, Sivasankaran S, Kim YJ. Effect of aspect ratio on convection in a porous enclosure with partially active thermal walls, Computers and Mathematics with Applications. 2011; 62:3844-3856.
5. Cheikh NB, Beya BB, Lili T. Influence of thermal boundary conditions on natural convection in a square enclosure partially heated from below, Int. Comm. Heat Mass Transfer, 2007; 34:369-379,
6. Mahmud S, Fraser RA. Magneto hydrodynamic free convection and entropy generation in a square porous cavity, Int. J Heat and Mass Transfer, 2004; 47:3245-3256,
7. Xu F, Saha SC. Transition to an unsteady flow induced by a fin on the sidewall of a differentially heated air-filled square cavity and heat transfer, Int. J. Heat and Mass Transfer, 2014; 71:236-244,
8. Prasad V, Kulacki FA. Connective heat transfer in a rectangular porous cavity - Effect of aspect ratio on flow structure and heat transfer, J. Heat Transfer, 1984; 106:158-165,
9. Varol Y, Öztop HF, Pop I. Numerical analysis of natural convection for a porous rectangular enclosure with sinusoidal, varying temperature profile on the bottom wall, Int. Comm. Heat Mass Transfer, 2008; 35:56-64,
10. Öztop HF. Natural convection in partially cooled and inclined porous rectangular enclosures, Int. J. Therm. Sci. 2007; 46:149-156,
11. Chamkha J, Ismael MA. Natural convection in differentially heated partially porous layered cavities filled with a nanofluid, Numer. Heat Transf. A Appl. vol. 2014; 65(11):113-1089,
12. Saied NH, Pop I. Non-Darcy natural convection in a square cavity filled with a porous media, Fluid Dynamics Research. 2005; 36:35-43,
13. Nithiarasu P, Seetharamu KN, Sundararajan T. Numerical investigation of buoyancy driven flow in a fluid saturated non-Darcian porous medium, Int. J. Heat and Mass Transfer, 1999; 42:1205-1215,

14. Rathish Kumar BV, Kumar B. Parallel computation of natural convection in trapezoidal porous enclosures, Mathematics and Computers in Simulation. 2004; 65:221-229,
15. Vafai K, Kim SJ. On the limitations of Brinkman–Forchheimer-extended Darcy equation, Int. J. Heat Fluid Flow. 1995; 16:11-15.
16. Zienkiewicz OC, Taylor RL. The finite element method Solid and Structural Mechanics, Sixth Ed., McGraw-Hill, 2005.
17. Khatun A, Rahman M, Alam S. Heat Transfer Characteristics of Nanofluid Due to a Permeable Rotating Disk with Slip Effect and Thermophoresis, Science & Technology Asia. 2019; 24(1):1-13,